Impact of Atmospheric Circulation Variability on U.S. Midwest Moisture Sources

THEO CARR[a,b] AND CAROLINE C. UMMENHOFER[b]

[a] *Massachusetts Institute of Technology–Woods Hole Oceanographic Institution Joint Program in Oceanography/Applied Ocean Science and Engineering, Cambridge and Woods Hole, Massachusetts*
[b] *Department of Physical Oceanography, Woods Hole Oceanographic Institution, Woods Hole, Massachusetts*

(Manuscript received 27 March 2023, in final form 3 October 2023, accepted 10 October 2023)

ABSTRACT: Elevated spring and summer rainfall in the U.S. Midwest is often associated with a strong Great Plains low-level jet (GPLLJ), which transports moist air northward to the region from the Gulf of Mexico. While the intensity of hourly precipitation extremes depends on local moisture availability and vertical velocity, sustained moisture convergence on longer time scales depends on horizontal moisture advection from remote sources. Therefore, the magnitude of moisture convergence in the Midwest depends in part on the humidity in these moisture source regions. Past work has identified the time-mean spatial distribution of moisture sources for the Midwest and studied how this pattern changes in years with anomalous rainfall. Here, using reanalysis products and an Eulerian moisture tracking model, we seek to increase physical understanding of this moisture source variability by linking it to the GPLLJ, which has been studied extensively. We find that on interannual time scales, an anomalously strong GPLLJ is associated with a shift in the distribution of moisture sources from land to ocean, with most of the anomalous moisture transported to—and converged in—the Midwest originating from the Atlantic Ocean. This effect is more pronounced on synoptic time scales, when almost all anomalous moisture transported to the region originates over the ocean. We also show that the observed positive trend in oceanic moisture contribution to the Midwest from 1979 to 2020 is consistent with a strengthening of the GPLLJ over the same period. We conclude by outlining how projected changes in a region's upstream moisture sources may be useful for understanding changes in local precipitation variability.

SIGNIFICANCE STATEMENT: In this work, we study how the origin of moisture that forms precipitation in the U.S. Midwest covaries with large-scale atmospheric circulation. Our results show that an intensification of the mean winds tends to increase the proportion of total rainfall that originates from the ocean. This analysis may help to constrain future projections of rainfall extremes in the central United States, as projected changes in humidity over the ocean are typically more robust and better understood than those over land.

KEYWORDS: Hydrologic cycle; Precipitation; Climate variability; Moisture/moisture budget; Teleconnections; North America

1. Introduction

Understanding the drivers of precipitation variability, including for extreme events, is necessary for assessing present-day risk and for forecasting possible increases in risk related to greenhouse gas emissions. This is particularly important in "breadbasket" regions, such as the U.S. Midwest, which produce a disproportionate amount of the world's food supply and are vulnerable to climate extremes (Hasegawa et al. 2022; Raymond et al. 2020). While energy-budget constraints provide a starting point for thinking about future changes in precipitation variability, regional differences from the global-mean change are expected to be significant and depend strongly on local circulation changes.

In the U.S. Midwest, summertime precipitation is strongly correlated with the strength of the Great Plains low-level jet (GPLLJ), which transports relatively warm, moist air to the region northward from the Gulf of Mexico. The GPLLJ's close association with precipitation—and extreme events in particular—has motivated numerous past studies of its variability and projected changes under warming scenarios (e.g., Zhou et al. 2022, 2021; Weaver and Nigam 2008; Higgins et al. 1997). While model-projected changes of the GPLLJ are fairly robust, those of Midwest precipitation, and its variability, are less certain (Bukovsky et al. 2017; Cook et al. 2008). In light of the uncertainties associated with these local factors, and the importance of horizontal moisture transport, it may be useful to take a Lagrangian perspective and focus on how upstream changes in the Midwest's moisture "source" regions (e.g., increasing specific humidity in the Gulf of Mexico) might impact moisture transport to, and precipitation in, the Midwest. In this study, we lay the groundwork for such an analysis by determining how the Midwest's moisture source regions depend on atmospheric circulation and, in particular, on the strength of the GPLLJ.

Located in the lower troposphere to the east of the Rocky Mountains, the time-mean GPLLJ can be considered part of the northward branch of the North Atlantic subtropical high (NASH) (Ting and Wang 2006; Rodwell and Hoskins 2001).

Supplemental information related to this paper is available at the Journals Online website: https://doi.org/10.1175/JCLI-D-23-0178.s1.

Corresponding author: Theo Carr, ktcarr@mit.edu

DOI: 10.1175/JCLI-D-23-0178.1

Positive anomalies in GPLLJ strength tend to converge moisture in the U.S. Midwest, which is located downstream of the GPLLJ's typical peak velocity, leading to the observed positive correlation between GPLLJ strength and Midwest precipitation on diurnal to interannual time scales.

On short time scales, GPLLJ anomalies are driven by the diurnal cycle and coupling with synoptic waves. The GPLLJ typically attains maximum wind speeds overnight, owing to 1) a nocturnal decoupling from the boundary layer and 2) the diurnal cycle of the zonal temperature gradient over the sloping foothills of the Rocky Mountains (Shapiro et al. 2016). While the time-average GPLLJ strength is about 5 m s^{-1} during summertime, speeds can reach 20 m s^{-1} overnight (Whiteman et al. 1997). The warm and moist air advected by these boundary layer–driven GPLLJs tends to destabilize the atmospheric column in the Midwest, often leading to pockets of localized convection and precipitation in the central United States (Tuttle and Davis 2006).

On slightly longer, synoptic time scales the GPLLJ frequently couples with upper-level circulation, including remotely forced jet stream meanders and locally generated mesoscale convective systems (Agrawal et al. 2021; Burrows et al. 2019; Feng et al. 2019; Pu and Dickinson 2014). These "coupled" GPLLJ events are more common in springtime, before onset of the North American monsoon inhibits baroclinic instability in the central United States, and typically generate much more precipitation than their boundary layer–driven counterparts (Wang and Chen 2009; Weng 2000). While a prototypical nocturnal jet is "uncoupled" from the upper-level circulation, coupled GPLLJs are associated with large-scale ascent between a cyclone–anticyclone pair (Bukovsky et al. 2017; Wang and Chen 2009).

On seasonal time scales, the strength of the GPLLJ is affected by persistent circulation anomalies forced by sea surface temperature anomalies in both the Atlantic and Pacific (Danco and Martin 2018; Krishnamurthy et al. 2015; Weaver et al. 2009) and by teleconnections related to the East Asian monsoon (Malloy and Kirtman 2022; Agrawal et al. 2021). These persistent circulation anomalies may affect moisture convergence in the Midwest "directly" by altering the mean flow component of the GPLLJ or "indirectly" by changing the frequency of baroclinic wave growth (and coupled GPLLJ events). In some cases, both mechanisms are important. For example, in 1993, an anomalously strong storm track in June and intensified GPLLJ in July led to devastating flooding in the central United States (Trenberth and Guillemot 1996; Bell and Janowiak 1995).

The intensity of such extreme events depends in part on atmospheric moisture availability. In the case of the central United States, the Gulf of Mexico and northwest Atlantic Ocean provide an "infinite" source of moisture from which individual storms and the GPLLJ can draw (Mo et al. 1997): at a velocity of 12 m s^{-1} (≈1000 km day^{-1}), the GPLLJ can transport moisture from the Gulf of Mexico to the U.S. Midwest in about a day (Trenberth 1999b). Estimates of how much of Midwest precipitation comes directly from the ocean may help to constrain future projections of precipitation intensity in the region, because changes in specific humidity over land are more uncertain than changes over the ocean (Byrne and O'Gorman 2018; Chadwick et al. 2016). Identifying precisely where this moisture comes from may also help to confirm links between sea surface salinity anomalies in the northwest Atlantic and precipitation in the U.S. Midwest (Li et al. 2022, 2018, 2016).

Past analyses based on moisture tracking models suggest that water vapor evaporating over the Gulf of Mexico and northwest Atlantic contributes substantially to precipitation in the central United States, and that moisture from these source regions is particularly important for extreme events, including the heavy rainfall in 1993 (Abel et al. 2022; Dirmeyer and Kinter 2010, 2009; Sudradjat et al. 2003; Brubaker et al. 2001). While this past work has pointed out that the GPLLJ links these oceanic source regions to the Midwest, an important unanswered question is how the time scale and "forcing mechanism" of GPLLJ anomalies impact the distribution of moisture sources.

To illustrate the importance of these factors, we draw on earlier examples: the GPLLJ is enhanced by (i) mesoscale convective systems on synoptic time scales and (ii) cool Atlantic sea surface temperature on seasonal time scales. While both mesoscale convective systems and a cool Atlantic strengthen the GPLLJ, the larger-scale circulation anomaly associated with each differs, affecting the origin of moisture advected into the Midwest. From a climate change perspective, the differing origin of this moisture may be important for projecting future precipitation variability, owing to a nonuniform pattern of warming (implying that specific humidity increases at different rates in each source region). This suggestion is motivated by recent work that finds that long-term changes in specific humidity in a particular land region can be predicted based on changes in specific humidity at the region's oceanic moisture sources (Byrne and O'Gorman 2018; Chadwick et al. 2016).

Independent of the forcing mechanism, time scale also matters because of the asymmetry between evaporation and precipitation: compared to the relatively slow and continuous process of evaporation, precipitation is fast and intermittent (Trenberth et al. 2011). While on synoptic time scales evaporation cannot balance a heavy precipitation event, on sufficiently long time scales—and in moisture-limited regions—evaporation and precipitation can be considered in balance, based on the Budyko framework (Roderick et al. 2014). One implication of this approximate balance between E and P is that long-term changes in circulation intensity alone would not affect the distribution of moisture sources (Chadwick et al. 2016). However, thermodynamic changes would: the fraction of precipitation originating from oceanic sources is projected to increase with warmer temperatures, as evaporation increases at a higher fractional rate over the ocean than over water-limited land regions (Gimeno et al. 2020; Findell et al. 2019). Changes in the pattern of circulation also matter: in the Midwest, the projected intensification of the GPLLJ during springtime may further increase the fraction of moisture originating from the ocean (Benedict et al. 2020).

In this study, we quantify the effect of GPLLJ anomalies on the distribution of the Midwest's moisture sources, with a focus on the impact of the time scale—and upstream "forcing

mechanism"—of the anomalies. In doing so, we seek to link understanding of GPLLJ *variability* with that of moisture sources for the central United States, extending past work that has noted the GPLLJ's importance in transporting oceanic moisture to the region. The remainder of the paper is structured as follows: in section 2 we describe the data and moisture tracking model used in this study, along with the index used to measure GPLLJ strength. In section 3 we present the results of our analysis, including a quantitative estimate of the moisture source anomalies associated with circulation variability on different time scales. In section 4, we discuss and interpret these results. Section 5 provides conclusions and an outlook for the study.

2. Materials and methods

a. Data

All data used in this study are from version 5 of the European Centre for Medium-Range Weather Forecasts reanalysis (ERA5; Hersbach et al. 2020), obtained at 1° horizontal resolution for the period 1979–2020. The E and P fields used by the moisture tracking model are obtained at 1-h intervals, while the u, v, and q fields used by the model are obtained at 3-hourly intervals and at 37 fixed pressure levels, ranging from 1000 to 1 hPa (the model is described in section 2b). Given that surface pressure deviates significantly from 1000 hPa (e.g., over the Rocky Mountains), we linearly interpolate this pressure-level data in the vertical to match the surface pressure, so that for every (x, y, t), there are 37 vertical levels ranging from the surface pressure to 1 hPa. We note that other authors have used a similar interpolation approach to run the same moisture tracking model with data at a much coarser vertical resolution (e.g., model output data with five vertical levels; Benedict et al. 2020). To ensure numerical stability for the moisture tracking model, we also upsample the ERA5 data in time by interpolating all fields to a time step of 6 min.

We focus our analysis on the months of April, May, and June (AMJ), even though the GPLLJ typically reaches peak intensity slightly later in the year (June–July). This choice is motivated by the higher frequency of baroclinic waves over the central United States prior to summertime monsoon onset: these waves often "couple" to the GPLLJ and lead to larger individual rainfall events compared to boundary layer–driven LLJs, which are more common after monsoon onset (Burrows et al. 2020; Weng 2000). While it is true that—in the seasonal mean sense—the correlation between the GPLLJ and Midwest rainfall is higher when both quantities are averaged over May–July (MJJ) instead of AMJ, springtime synoptic events can indirectly impact summer rainfall by increasing soil moisture in the Midwest and southern United States (Li et al. 2016). For example, past work partially attributed summertime Midwest flooding in July and August 1993 to a high frequency of synoptic GPLLJ events in June (Trenberth and Guillemot 1996; Bell and Janowiak 1995). Ultimately, the results of our analysis are qualitatively unchanged if performed on MJJ or June–August (JJA) instead of AMJ (figures not shown).

b. Moisture tracking model

In this work, we apply a moisture tracking algorithm to estimate moisture sources for the U.S. Midwest based on ERA5. The moisture tracking model we use is the two-layer "Water Accounting Model" (van der Ent 2019; van der Ent et al. 2014). This model uses the horizontal velocity and specific humidity fields (u, v, and q, respectively) from the reanalysis to trace water vapor from a specified sink region backward in time, and attempts to estimate the water vapor's "source" location (where it most recently evaporated from the surface). While the model does not place any constraints on the time scale of the backward tracking, past work using age tracers has found the average time elapsed between evaporation from a source region and subsequent precipitation in a sink region is on the order of 8–12 days in the model (van der Ent and Tuinenburg 2017; van der Ent et al. 2014). For our study, the sink region is chosen as the upper Midwest, outlined by a dashed white line in Fig. 1a. This region is chosen because its precipitation is strongly affected by the GPLLJ (Fig. 2) and may be impacted by future changes in the position of the GPLLJ (Cook et al. 2008).

The model is based on the atmospheric budget for precipitable water (Trenberth and Guillemot 1995):

$$\frac{\partial w}{\partial t} = -\nabla \cdot \frac{1}{g}\int_0^{p_s} q\mathbf{u}\, dp + E - P \tag{1}$$

where $w = (1/g)\int_0^{p_s} q\, dp$ is the mass of precipitable water in an atmospheric column (units: kg m^{-2}), q is specific humidity, $\mathbf{u}$ is the horizontal velocity, p_s is the surface pressure, and $(1/g)\int_0^{p_s} q\mathbf{u}\, dp$ is the vertically integrated moisture flux. Denoting *tracked* precipitable water (or "tracked moisture") from the sink region as $\tilde{w}$, a one-layer version of the moisture tracking model integrates the following "weighted" form of the precipitable water budget backward in time:

$$\frac{\partial \tilde{w}}{\partial t} = \frac{\tilde{w}}{w}\left[-\nabla \cdot \frac{1}{g}\int_0^{p_s} q\mathbf{u}\, dp + E\right] - \tilde{P}, \tag{2}$$

where $\tilde{P}(x, y) = P(x, y)$ if (x, y) is in the sink region, and zero otherwise. In this one-layer model, the rate at which a given grid cell contributes to precipitation in the sink region—the "tracked evaporation" rate—is given by the weighted evaporation term in Eq. (2), $\tilde{E} = (\tilde{w}/w)E$. To account for vertical shear, we use a two-layer version of this model, in which we split the vertical integral of precipitable water and moisture fluxes into two pressure regions. For example, we define $w_1 = (1/g)\int_{p_b}^{p_s} q\, dp$ as the lower-level precipitable water and $w_2 = (1/g)\int_{p_b}^{p_s} q\, dp$ as the upper-level precipitable water, where p_b is the pressure at the boundary between the two layers (approximately 800 hPa in regions near sea level; see Fig. S1 in the online supplemental material for a detailed map). A detailed explanation of the two-layer formulation is provided in appendix A.

To reduce computation time, the moisture tracking model was run in parallel on each year of ERA5 data from 1979 to 2020 (such that the model tracked moisture backward in time from 31 December to 1 January for each calendar year).

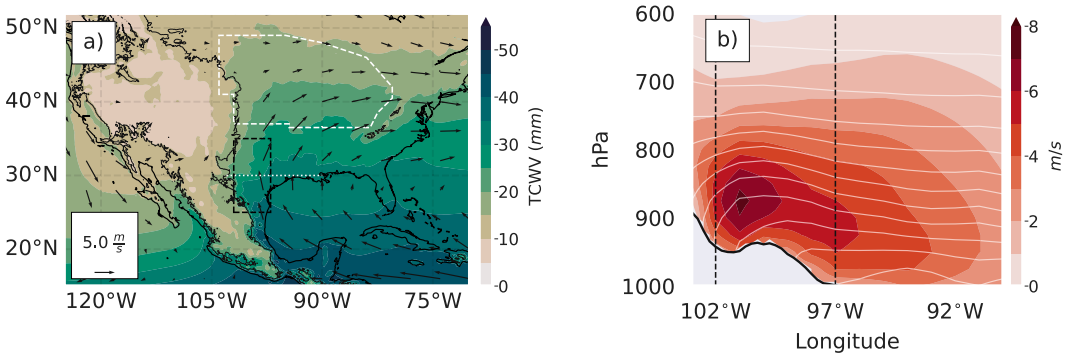

FIG. 1. Moisture transport in the continental United States, in April, May, and June (AMJ). (a) Total column water vapor (colors) and 850-hPa horizontal winds (vectors). Black line in the western United States is the 1000-m contour of topography. Dashed black rectangle outlines the GPLLJ region, dashed white line outlines the Midwest region, and dotted white line indicates location of cross section shown in (b). (b) Vertical structure of meridional wind and specific humidity, along the cross section indicated by the dotted white line in (a). Colors indicate meridional velocity, and white contours indicate specific humidity (1 g kg^{-1} contour interval). The maximum contour value, located adjacent to the surface, is 13 g kg^{-1}.

Therefore, there is some model "spinup" associated with precipitation near the start of a given calendar year which evaporates in the previous calendar year. Because the model typically tracks moisture backward in time for 8–12 days (van der Ent and Tuinenburg 2017; van der Ent et al. 2014), this spinup mainly impacts moisture source estimates for the month of December. Because the total spinup error is small (<2%, based on the residual between precipitation in the sink region and tracked evaporation integrated over the globe) and concentrated at the end of the calendar year, it should not affect our main results, which focus on the months of April, May, and June.

c. *GPLLJ indices*

To quantify the strength of the GPLLJ, we define a GPLLJ index based on the average meridional wind at 850 hPa in the region bounded by 25°–35°N, 102°–97°W, similar to Malloy and Kirtman (2020) and Weaver and Nigam (2008). This region is outlined by the black dashed rectangle in Fig. 1a. We compute the area average based on 3-hourly data, then resample to daily or monthly data as necessary by averaging in time.

In parts of the analysis, we also consider composites of GPLLJ "events." Events are defined as days where the GPLLJ index exceeds its mean value plus one standard deviation. To facilitate comparison with recent studies investigating large-scale coupling of the GPLLJ, we also use a different metric to classify daily GPLLJ events into "coupled" and "uncoupled" events. Specifically, we use the methodology described by Burrows et al. (2019): first, we determine whether a given day has a jet event by computing the difference in meridional wind between 850 and 700 hPa in the jet region. If the jet meets a minimum shear criterion, the event is classified as coupled or uncoupled based on the local wave activity to the west of the jet region. Local wave activity is computed based on geopotential height at 500 hPa, using Eqs. (2) and (3) from Martineau et al. (2017).

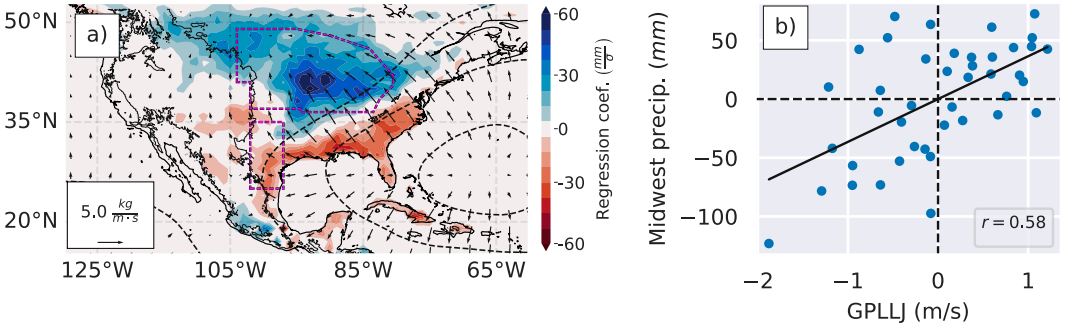

FIG. 2. Covariance of seasonal-mean GPLLJ strength and precipitation, for AMJ. (a) Spatial distribution of precipitation and circulation anomalies, obtained by linearly regressing spatial fields onto the AMJ-averaged GPLLJ index (defined in section 2c). Colors show coefficients for precipitation, vectors show coefficients for the divergent component of vertically integrated moisture flux, and contours show coefficients for vertically integrated moisture flux potential at intervals of 2×10^6 kg m^{-2} s^{-1}. (b) Scatterplot of GPLLJ strength vs Midwest precipitation summed over AMJ, for the period 1979–2020 (each point represents a single year). Correlation coefficient is $r = 0.58$ ($p < 0.01$).

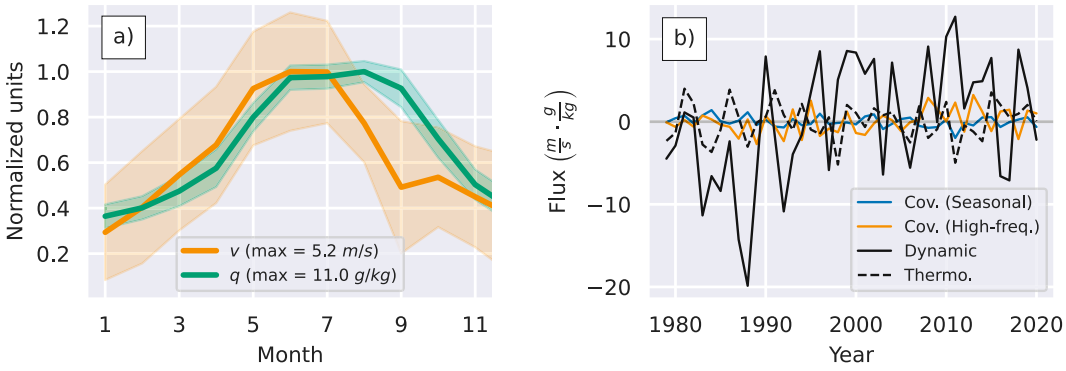

FIG. 3. Relative importance of dynamic and thermodynamic components of moisture flux, in the GPLLJ region. (a) Annual cycle of 850-hPa meridional velocity (v_{850}) and specific humidity (q_{850}), averaged over the GPLLJ region (outlined by dashed black rectangle in Fig. 1a). Solid line indicates the mean and shading indicates ±1 standard deviation. Both curves have been normalized by their respective maximum values, which are specified in the legend. (b) Dynamic and thermodynamic contributions to 850-hPa moisture flux anomalies in the GPLLJ region during AMJ. The seasonal anomaly is separated into four components, representing 1) dynamic, 2) thermodynamic, 3) monthly covariance, and 4) high-frequency covariance contributions (see appendix B for details of the decomposition).

d. Significance testing

For several of the results presented in the following section (Figs. 5c,d, 6e–g, and 8c), we use a Monte Carlo approach to assess statistical significance. To estimate the distribution of possible results due to random chance, we draw 1000 random samples then compute the upper and lower 2.5% percentiles, corresponding to a 95% confidence interval. For regression coefficients (Figs. 5c,d and 8c), samples are drawn by randomly shuffling the data in time and fitting a regression line. For composites (Figs. 6e–g), samples are drawn by averaging the data over a randomly chosen set of times (selected with replacement).

3. Results

In this section, we characterize the climatology and variability of the GPLLJ most relevant to this study (section 3a), quantify the effect of seasonal and synoptic circulation variability on moisture sources (sections 3b and 3c), and analyze observed long-term changes in moisture sources (section 3d).

a. Large-scale circulation and GPLLJ variability

Before discussing how circulation variability impacts the distribution of moisture sources for the Midwest, we provide a brief overview of the time-mean circulation and anomalies associated with GPLLJ variability. Figure 1a shows the time-mean total column water vapor (colors) and 850-hPa winds (vectors) over the continental United States during April–June, while Fig. 1b shows a cross section of the meridional wind (colors) and specific humidity (contours) along the dotted white line at 30°N in Fig. 1a. The GPLLJ appears in Fig. 1b as the maximum in wind speed along the sloping topography (centered near 100°W and 850 hPa).

When the GPLLJ is anomalously strong, moisture flux through the Midwest's southern boundary increases, often leading to moisture convergence and precipitation in the Midwest. This is depicted in Fig. 2a, which shows anomalies for precipitation (colors) and the divergent component of vertically integrated moisture flux (vectors) associated with a one standard deviation increase in GPLLJ strength. Owing to this relationship, seasonal-mean GPLLJ strength is a fairly strong predictor of seasonal-mean rainfall in the Midwest (Fig. 2b).

GPLLJ intensity (as measured by our GPLLJ index) exhibits strong seasonality, growing in strength through the spring before reaching peak intensity in May–July (Fig. 3a). This springtime intensification reflects the annual expansion of the NASH during the same period. Specific humidity averaged over the GPLLJ region (also at 850 hPa) exhibits a similar, though slightly lagged, seasonal cycle, peaking from June to August (Fig. 3a).

While the wind-based GPLLJ index does not account for specific humidity, it serves as a good proxy for moisture flux in the GPLLJ region. To show this, we decompose the seasonal-mean 850-hPa moisture flux in the GPLLJ region, $(\overline{vq})_{850}$, into four components representing 1) dynamic contributions from seasonal-mean anomalies in wind speed, 2) thermodynamic contributions from seasonal-mean anomalies in specific humidity, 3) covariance of seasonal anomalies, and 4) covariance of high-frequency eddies (see appendix B for a derivation). Consistent with past work (Li and Li 2015), we find that variance of the seasonal mean moisture flux in the GPLLJ region is dominated by the dynamic component (Fig. 3b). The dominance of dynamic over thermodynamic anomalies can be understood by considering the ratio of the standard deviation to the mean for humidity and velocity in the GPLLJ region. As shown in Fig. 3a, interannual variability of wind speed—as a fraction of the mean value—is much larger than that for specific humidity. The dominance of dynamic anomalies implies that our wind-based GPLLJ index is an effective proxy for moisture transport.

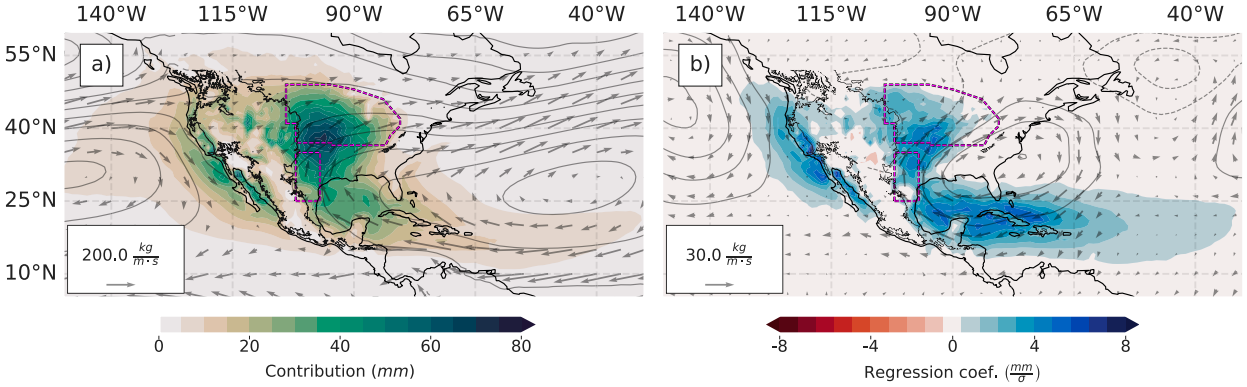

FIG. 4. Spatial distribution of moisture sources for the U.S. Midwest during AMJ. (a) Climatology of moisture sources, summed over AMJ months. Color indicates the amount of Midwest precipitation which originated from a given location. Also shown for context are vertically integrated moisture flux (vectors) and 850-hPa geopotential height (open contours; maximum value of 1560 gpm and interval of 20 gpm). (b) Moisture source anomalies associated with a one standard deviation increase in GPLLJ strength during AMJ. Obtained by linearly regressing the AMJ moisture source anomalies for each year onto the AMJ-averaged GPLLJ index. Regression coefficients for vertically integrated moisture flux and Z_{850} are also shown (contour interval: 2 gpm).

b. *Moisture sources for the U.S. Midwest on seasonal time scales*

In AMJ, evaporative fluxes from land and ocean surfaces contribute comparable amounts to precipitation in the U.S. Midwest. This is illustrated in Fig. 4a, which shows the climatological distribution of moisture sources (geopotential height and vertically integrated moisture flux are also shown for context). Figure 4a indicates that much of the Midwest's precipitation during these months evaporates in the central United States, with the highest rates of moisture contribution located just south of the outlined Midwest region, near 35°N, 95°W. As expected, the Gulf of Mexico and northwest Atlantic Ocean also contribute substantial moisture, as moisture is advected westward and northward by the anticyclonic circulation of the NASH (identified as the local maximum in geopotential height over the Atlantic Ocean in Fig. 4a).

When the GPLLJ is strong, as measured by the GPLLJ index, both ocean and land tend to contribute more moisture than in the time-mean case (consistent with an increase in Midwest precipitation), but the ocean contributes a larger fraction of the total. This is illustrated in Fig. 4b, which shows the spatial distribution of moisture sources linearly regressed onto the GPLLJ index for AMJ. Overlaid coefficients for geopotential height and vertically integrated moisture flux show that a strong GPLLJ is associated with a broader circulation anomaly that advects moisture from the Gulf of Mexico and Caribbean Sea into the continental United States. While the regression coefficients for moisture sources (colors) are positive almost everywhere—indicating increased moisture contribution—the spatial pattern differs from that of the climatology (cf. colors in Figs. 4a,b). In particular, compared to the climatology 1) a larger fraction of the anomalous moisture originates from the Gulf of Mexico and Caribbean Sea and 2) a smaller fraction originates over land. One way to think about this shift in the distribution of moisture sources is that air parcels advected from the Atlantic to the Midwest at higher velocities have less time to "absorb" moisture evaporating from land, assuming evaporation rates are near-constant (see appendix C for a quantitative argument). In turn, the fractional increase in moisture contribution from the Pacific is not as large as the Atlantic owing to the relatively weak circulation anomalies in the Pacific and western United States.

To clarify this point, we plot the spatially integrated moisture contributions from land and ocean regions in Fig. 5. In the time mean, moisture sourced from the ocean is the dominant contributor to Midwest precipitation in boreal winter, while land surfaces contribute most moisture in late summer (cf. blue and green lines in Fig. 5a). Note that the dominance of oceanic moisture sources in winter likely results from reduced evaporation over land surfaces during the cold months and relatively large evaporative fluxes over the ocean (e.g., resulting from cold continental air flowing over relatively warm water; Trenberth 1999a). In the case of the Midwest, most of the moisture contributing to wintertime precipitation comes from the Pacific, likely via synoptic systems that advect moisture over the western United States and Mexico. This interpretation is supported by Fig. 5b, which shows the seasonal cycle of moisture contributed to Midwest precipitation by the Pacific and Atlantic. The Pacific's peak contribution in March, April, and May occurs before onset of the summertime monsoon inhibits baroclinic instability (and growth of synoptic systems). The Atlantic's contribution peaks slightly later, from about May to July, consistent with the peak strength of the GPLLJ (cf. Fig. 3a). Note that the variance for the Atlantic-derived moisture (indicated by shading) is large compared to Pacific-derived moisture, particularly in summer, suggesting its importance for extreme events. The overlap of the large Pacific and Atlantic contributions in May leads to the overall peak in oceanic moisture contribution during this month (blue curve in Fig. 5a).

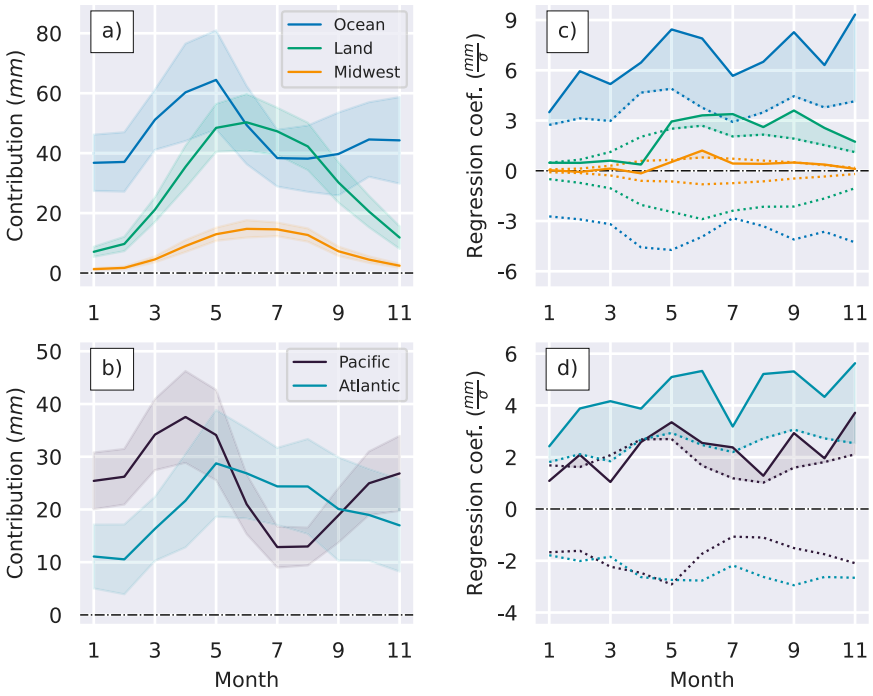

FIG. 5. Seasonal cycle of ocean and land moisture sources for the U.S. Midwest. (a) Seasonal cycle of moisture sources for the Midwest, integrated over ocean, land, and the Midwest region (the latter is a subset of the "land" contribution). Solid lines indicate mean quantities, while shading indicates ±1 standard deviation. (b) As in (a), but for the Atlantic and Pacific Oceans (both subsets of the "ocean" contribution). (c) Spatially integrated moisture source anomalies associated with a one standard deviation increase in GPLLJ strength, obtained by linearly regressing the anomalies for each month onto the GPLLJ index (computed separately for each month). Shading fills the region between the 95% confidence threshold (dotted lines) and composite, indicating statistical significance. (d) As in (c), but for moisture source anomalies integrated over the Atlantic and Pacific Oceans. In all panels, results for December are omitted because of model spinup.

As noted previously, a strong GPLLJ is associated with an increase in the fraction of moisture contributed by the ocean. This is clearly illustrated in Fig. 5c, which shows the spatially integrated moisture sources from Fig. 5a linearly regressed onto the GPLLJ index (regression coefficients computed separately for each month). While the ratio of ocean-to-land moisture contribution during April, May, and June is typically on the order of 1–1.5 (cf. blue and green curves in Fig. 5a), the ocean contributes 2–3 times more of the anomalous moisture associated with an anomalously strong GPLLJ in May and June, and almost all of the anomalous moisture in April (cf. blue and green curves in Fig. 5c). Similar ratios are observed for other months, including in mid-to-late summer, when moisture contributed from land typically dominates. Note that most of the anomalous oceanic moisture associated with GPLLJ events comes from the Atlantic, even in the winter and early spring when the Pacific Ocean typically contributes more moisture (cf. Figs. 5b and 5d). While the GPLLJ may couple to baroclinic systems which advect moisture from the Pacific, it is a more direct proxy for moisture advected from the Gulf of Mexico and Atlantic Ocean.

c. *Moisture sources for the U.S. Midwest linked to GPLLJ variability and synoptic waves*

On shorter time scales the GPLLJ often couples to synoptic waves, and the associated anomalous precipitation is sustained by an even larger fraction of oceanic moisture as compared to seasonal time scales. This coupling can be seen by compositing the upper-level geopotential height fields on days where the GPLLJ is strong (Figs. 6a–d). Read from top to bottom, Figs. 6a–d show the 200-hPa geopotential height anomalies (open contours) and tracked moisture anomalies (colors) from 4 days before a GPLLJ event to 2 days after an event. This upper-level wave pattern has been noted in previous studies of GPLLJ variability (e.g., Burrows et al. 2019; Mo et al. 1997) and resembles the stationary wave pattern associated with the East Asian monsoon (Agrawal et al. 2021). As the wave propagates across North America (Fig. 6c), it advects anomalous moisture from the Gulf of Mexico and Pacific Ocean into the United States, where the moisture precipitates out of the atmosphere (precipitation anomalies are shown in Fig. S2).

We estimate the moisture source regions for the anomalous precipitation by compositing the spatially integrated moisture

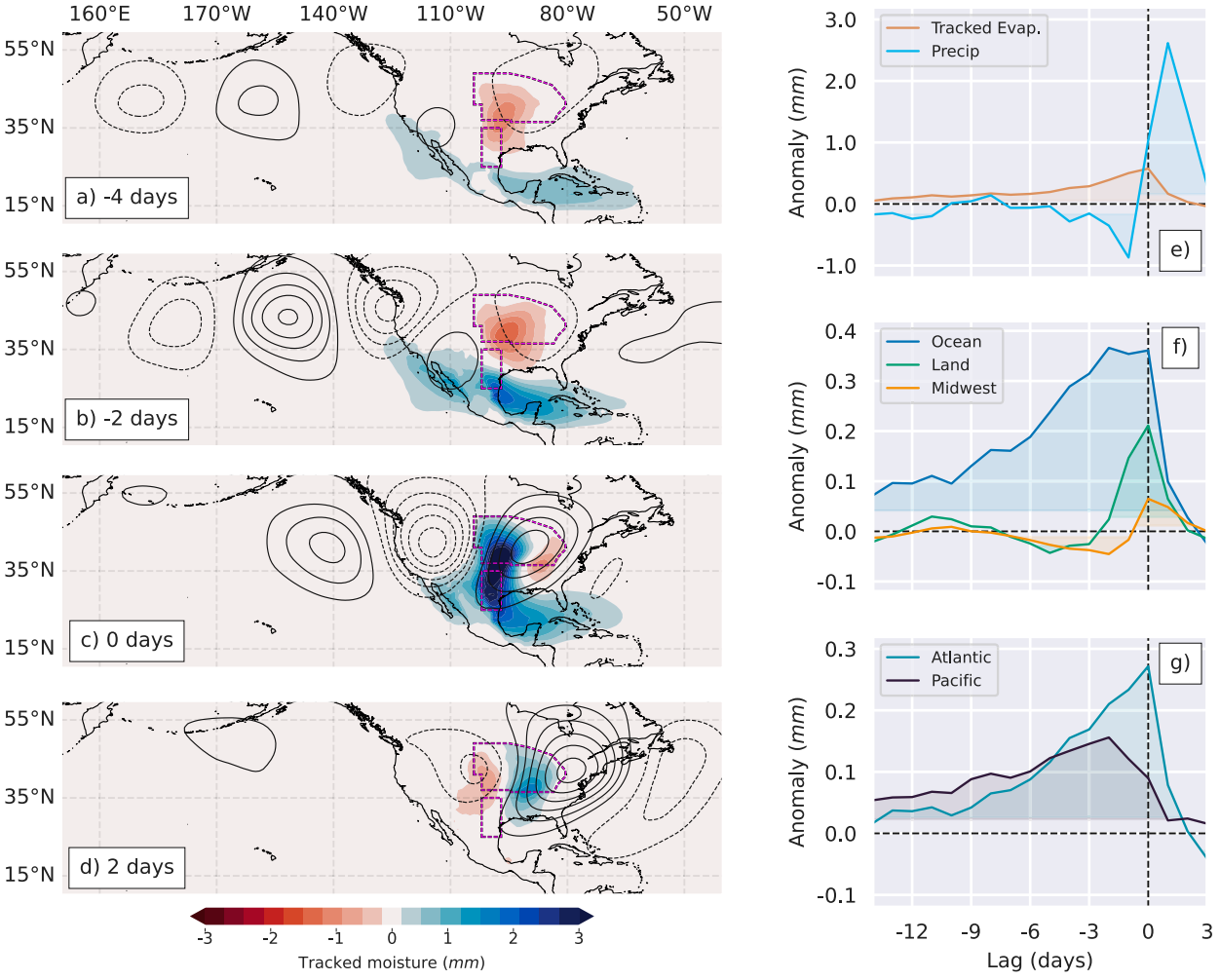

FIG. 6. Moisture transport associated with synoptic GPLLJ variability in AMJ. (a)–(d) Composite anomalies of tracked moisture (colors) and Z_{200} (open contours; interval of 10 gpm) from 4 days before a GPLLJ event to 2 days after an event. GPLLJ events are defined as days when the daily-averaged index exceeds its mean value plus one standard deviation (about 600 days, or ~16% of all AMJ days between 1979 and 2020). (e) Composite anomalies of Midwest precipitation and globally integrated tracked evaporation from 14 days before a GPLLJ event to 3 days after an event. Shading indicates statistical significance at the 95% confidence level, obtained via bootstrap random sampling (details provided in Methods section). (f),(g) As in (e), but for different components of the tracked evaporation, as in Fig. 5.

sources from 14 days before a GPLLJ event to 3 days after an event. This approach is validated by evaluating the balance between Midwest precipitation and the global integral of moisture sources ("tracked evaporation") over the same interval. Note that over sufficiently long time periods (relative to the residence time of water in the atmosphere), the integral of these curves is approximately equal (by design of the moisture tracking model). As shown in Fig. 6e, there is a large and positive Midwest precipitation anomaly following the composite GPLLJ event, which is balanced by a relatively small, positive evaporation anomaly that persists over the preceding two weeks. This asymmetry is expected—evaporation is a continuous process, while precipitation is intermittent and occurs at much higher rates over much shorter time intervals (Trenberth et al. 2011)—and provides further evidence that most moisture contributing to synoptic precipitation in the Midwest is already in the atmosphere several days prior to the event (Trenberth 1999b). While use of an Eulerian moisture tracking model means we cannot unequivocally attribute the positive precipitation anomaly to the preceding evaporation anomalies, the time scale of the evaporation anomaly matches that of typical atmospheric residence times for water vapor (5–10 days), and the area under the two curves integrated over this 17-day period is the same order of magnitude, providing some confidence in the approach's utility.

Having established the link between the anomalous precipitation and tracked evaporation shown in Fig. 6e, we find that almost all of this anomalous evaporation occurs over the ocean. This can be seen in Fig. 6f, which shows the breakdown of the globally integrated tracked evaporation into integrals over land, the ocean, and the Midwest region (just as in Figs. 5a,c). Most of the anomalous oceanic moisture is contributed by the Atlantic, as shown in Fig. 6g. However, the discrepancy between the Atlantic and Pacific contributions

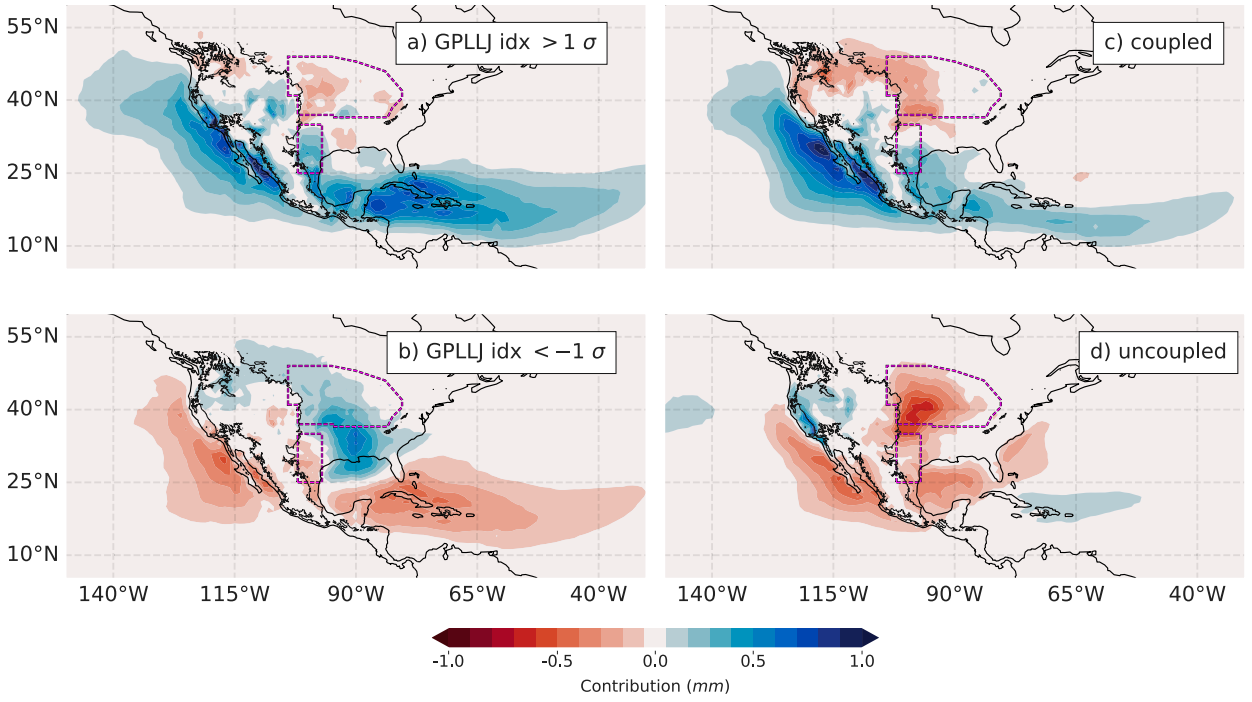

FIG. 7. Moisture source anomalies composite of daily GPLLJ events obtained by summing tracked evaporation from 14 days before a GPLLJ event to 2 days after a GPLLJ event. Different panels correspond to different definitions of a GPLLJ event. (a) Days when GPLLJ index exceeds +1 standard deviation (this is the same definition used in Fig. 6) and (b) days when GPLLJ index is less than −1 standard deviation [shown for context to illustrate asymmetry with (a)], as well as (c) "coupled" and (d) "uncoupled" GPLLJ events.

is smaller than it is on seasonal time scales (cf. Figs. 6g and 5d). The relatively high Pacific contribution on shorter time scales might be explained by the greater importance of upper-level coupling: as depicted in Fig. 6c, the same upper-level circulation which enhances the GPLLJ on synoptic time scales tends to advect moisture from the Pacific.

To provide further evidence that upper-level coupling increases moisture transport from the Pacific, we reproduce the composites shown in Fig. 6 for coupled and uncoupled GPLLJ events in Figs. S3 and S4, respectively. In the coupled case (Fig. S3g) most of the anomalous evaporation is contributed by the Pacific, while in the uncoupled case (Fig. S4g) there is almost no anomalous evaporation from the Pacific. For easier comparison between different types of GPLLJ events, we also integrate the spatial moisture source composites in time from 14 days before a GPLLJ event to 2 days after an event, shown in Fig. 7.

d. Trends in U.S. Midwest moisture sources

As discussed in the introduction, the GPLLJ is projected to intensify during the spring season under future warming scenarios, due to a northwest-ward shift of the NASH (Zhou et al. 2022, 2021; Cook et al. 2008). There is also some observational evidence for a GPLLJ intensification in the AMJ months for the period 1979–2012 (Barandiaran et al. 2013), possibly resulting from an expansion of the NASH over the same period (Li et al. 2011). This observed increase in GPLLJ strength is accompanied by an increase in the contribution of oceanic moisture sources to Midwest precipitation over the same interval, as shown in Fig. 8a, although the trends are barely significant at the 95% confidence level (black and blue curves during AMJ in Fig. 8c). In contrast, the trend in moisture contributions from land surfaces is close to zero during AMJ (green curves in Figs. 8b,c).

The relatively strong covariance between GPLLJ strength and oceanic moisture contribution discussed in section 3b ($r = 0.62$, $p < 0.01$ after detrending)—especially as compared to that between GPLLJ strength and moisture sourced from land surfaces ($r = 0.37$, $p = 0.02$)—suggests that the positive trends for each quantity are not purely coincidental. That is, the strong covariance suggests that circulation changes have caused the increased oceanic moisture contributions to Midwest rainfall. Such a circulation-driven increase differs from the thermodynamic-driven increase expected in a warmer climate, which results from larger increases in evaporation rates over the ocean (Findell et al. 2019). This thermodynamic effect is likely negligible over our relatively short analysis period; as evidence, we find that the trend in 850-hPa specific humidity in the GPLLJ region is close to zero over the period 1979–2020, such that the positive trend in moisture flux averaged over the GPLLJ region (not shown) is driven by dynamic rather than thermodynamic changes.

4. Discussion

Past work has shown that on seasonal time scales, large precipitation anomalies in the U.S. Midwest are sustained by oceanic moisture transported to the region by the GPLLJ (e.g.,

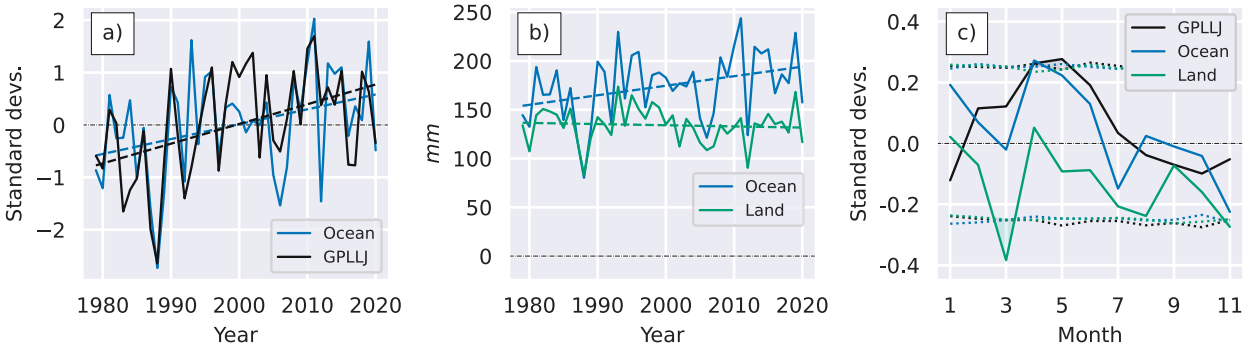

FIG. 8. Linear trends in GPLLJ and moisture sources. (a) GPLLJ strength and oceanic moisture contribution during AMJ, over time (both quantities have been normalized by their standard deviation). After detrending, correlation coefficient is $r = 0.62$ ($p < 0.01$). Dashed lines show the linear best-fit for each quantity. (b) Absolute (nonnormalized) moisture contribution from ocean and land sources during AMJ, over time. (c) Trend in GPLLJ strength (black line), oceanic contribution to Midwest precipitation (blue line), and land contribution to Midwest precipitation (green line), computed separately for each month of the year. Dotted lines show the 95% confidence bounds for each quantity. For AMJ, the linear trend for GPLLJ strength is 0.32 m s^{-1} $decade^{-1}$, while the linear trends for moisture contributions from ocean and land are 10 and -1.2 mm $decade^{-1}$, respectively. In (c), results for December are omitted because of model spinup.

Dirmeyer and Kinter 2010; Dirmeyer and Brubaker 2007; Brubaker et al. 2001), but has not explicitly considered how the time scale (and "forcing mechanism") of GPLLJ variability impacts the origin of this moisture. Here, we address this question by quantifying the Midwest moisture source anomalies associated with GPLLJ variability on different time scales. In doing so, we link understanding of GPLLJ variability, which is relatively well studied, with that of moisture sources for the central United States. Our analysis may also help to constrain future projections of precipitation variability in the central United States, as projected changes in specific humidity over the ocean and circulation are more robust than projections of precipitation over land.

Our results should be interpreted in the context of the ERA5 uncertainty and the moisture tracking model's limitations. With regards to the reanalysis, ERA5 does not assimilate evaporation observations and only assimilates composite radar–rain gauge precipitation estimates in the United States starting in 2009 (Lavers et al. 2022; Lopez 2011). While past work has not explicitly assessed how these errors might impact moisture-tracking estimates, it has demonstrated that hydrological models perform worse when forced by ERA5 than when forced by rain gauge data in the central and eastern United States, where the network of observations is relatively dense (Tarek et al. 2020). One well-known issue is that ERA5 has a slight negative precipitation bias in the central United States during summertime, possibly because the reanalysis does not model irrigation and because it poorly represents convective precipitation, which is more frequent in the warm months (Lavers et al. 2022).

To assess the magnitude—and potential impact on our results—of evaporation and precipitation biases in ERA5, we compare each field to an "independent" dataset: for precipitation, we compare daily and monthly ERA5 estimates to those from the Parameter-Elevation Regressions on Independent Slopes Model (PRISM), which is based on interpolation of weather station data (Di Luzio et al. 2008); and for evaporation, we compare monthly ERA5 estimates to those from the Global Land Evaporation Amsterdam Model (GLEAM), a prognostic model that assimilates satellite observations of soil moisture (Martens et al. 2017; Miralles et al. 2011).

In the time-mean sense, there is only a small difference between ERA5 and PRISM estimates of Midwest precipitation during AMJ. The difference between ERA5 and GLEAM estimates of evaporation is much larger, on the order of 25% (Fig. S6). The large difference does not necessarily indicate that ERA5 is biased, given that the GLEAM dataset has its own errors and uncertainties; for example, Dong et al. (2022) found that ERA5 estimates actually agreed better with observations from 14 flux tower sites in North America than GLEAM did. Instead, the large difference between the datasets should be interpreted as one (crude) measure of the ERA5 evaporation uncertainty. This uncertainty applies to our estimates of the relative importance of time-mean moisture contributions from ocean versus land (i.e., Figs. 4a and 5a,b).

After detrending, agreement between ERA5 and PRISM precipitation estimates is robust (Fig. S7). While agreement between ERA5 and GLEAM evaporation estimates is weaker (Fig. S8), the variance of evaporation is much smaller than that of precipitation (about 75% less), meaning that errors for each variable are of similar magnitude (cf. magnitude of errors plotted in Figs. S7b and S8b). These errors—differences between the datasets after detrending—are unlikely to bias our estimates of how circulation variability impacts the distribution of moisture sources, because they are only weakly correlated with the GPLLJ index. To the extent that such a bias does exist, it would cause the moisture tracking model to overestimate the fraction of total moisture contributed by land surfaces to Midwest precipitation when the GPLLJ is strong (because the model "sees" evaporation rates that are too large over land as parcels from the Midwest are advected backward in time).

With regard to the moisture tracking model, a crude parameterization of vertical motion and coarse horizontal resolution introduce potential biases, particularly relating to moisture

fluxes in the vicinity of topography. While a past study found that this two-layer tracking model yielded similar results to three-dimensional "online" moisture tracking in a GCM (van der Ent et al. 2013), this analysis was based on a study region in West Africa, which lacks topography comparable to the Rocky Mountains. In particular, one likely bias of the moisture tracking model is an overestimation of the Pacific Ocean's moisture contribution to the Midwest. This may result from numerical diffusion of the relatively large zonal moisture gradient on the eastern slopes of the Rockies (cf. Fig. 1a). Intuitively, the moisture tracking model cannot discern the exact location of moisture at subgrid scales, such that too much tracked moisture is assigned to the "dry" side of the gradient, and tracked backward across the dry region until it reaches a region with higher evaporation rates (Gimeno et al. 2012).

While this numerical error may bias our results, the direct moisture flux across the Rocky Mountains is relatively large during synoptic GPLLJ events, at least as represented in ERA5 (see Figs. S2 and S9). This is consistent with past studies that have found that cross-Rocky moisture fluxes contribute meaningfully to precipitation in the central United States (Benedict et al. 2020; Wang and Chen 2009). To bolster confidence in the results presented here, we provide a quantitative argument for why numerical dissipation across the Rocky Mountains would act to *decrease* the apparent importance of the Atlantic moisture source relative to moisture evaporating from land in appendix C. Confidence in our results could be increased further by rerunning the moisture tracking model with higher-resolution input data (e.g., 0.25° ERA5 data) or by directly comparing our results with those from a different type of tracking algorithm, such as a Lagrangian (trajectory-based) model. Notably, a Lagrangian model—as used by Algarra et al. (2019)—would be better suited to identify the moisture sources for synoptic precipitation events.

5. Conclusions and outlook

In summary, we find that on interannual time scales, positive GPLLJ anomalies are associated with increased moisture contribution from all source regions, with an increase in the fractional contribution of the ocean, and the Atlantic in particular (Figs. 4b and 5c,d). On synoptic time scales, this shift is more pronounced, with almost all anomalous moisture coming from oceanic sources (Figs. 6f and 7a), and roughly equivalent fractions coming from the Atlantic and Pacific (Fig. 6g).

On synoptic time scales, the increased importance of Pacific moisture in particular likely results from upper-level Rossby waves, which advect moisture eastward over the western United States and Mexico to the central United States while also intensifying the GPLLJ. The increased importance of oceanic moisture more generally on these time scales likely results from the relative slowness of evaporation compared to precipitation. Local atmospheric moisture cannot sustain prolonged heavy precipitation events and cannot be replenished by evaporation on the time scales of extratropical synoptic systems, implying that remote sources (including the ocean) must supply additional moisture.

On interannual time scales, the increased importance of oceanic transport from the Atlantic compared to the Pacific may result from the Atlantic-based forcing mechanism for GPLLJ variability: namely, a westward expansion of the NASH, which is associated with anomalously cold sea surface temperature in the Atlantic (e.g., Wang and Lee 2007). This is inferred from the relatively weak westerly moisture flux over the eastern Pacific and western United States in the interannual case (cf. Fig. 4b to the synoptic case in Figs. 6b,c). The high correlation between NASH extent and GPLLJ strength provides further evidence for the importance of Atlantic-based variability on interannual time scales (Fig. S5).

More generally, the less-drastic increase in oceanic moisture sources associated with interannual GPLLJ variability (cf. Figs. 5c and 6f) likely results from land–atmosphere feedbacks. On sufficiently long time scales, evaporation anomalies can be approximated to scale with precipitation anomalies using the Budyko framework (Roderick et al. 2014). In moisture-limited regions, the relationship is approximately linear, such that $E \approx \alpha P$ for some constant α. Assuming P scales with the vertical flux of specific humidity ($P \sim Mq$), and the vertical mass flux scales with low-level mass divergence ($M \sim -\nabla \cdot \mathbf{u}$), then evaporation can be approximated to scale as $E \approx \alpha P \sim \alpha(Mq) \sim -\alpha q(\nabla \cdot \mathbf{u})$ (Chadwick et al. 2016). This implies that on sufficiently long time scales, evaporation over land approximately scales with low-level mass divergence, which in turn scales with low-level velocity.

Therefore, to the extent that a strengthening of the GPLLJ represents a uniform intensification of the "upstream" velocity field (i.e., the paths along which air parcels are advected to the Midwest), we would expect a positive GPLLJ anomaly to increase moisture contribution from all sources equally on long time scales, leading to an amplification of the climatological moisture sources shown in Fig. 4a. While a positive GPLLJ anomaly on interannual time scales *does not* represent a uniform intensification of the large-scale velocity field (cf. Figs. 4a,b), much of the moisture advected into the Midwest indeed passes through the southern United States, in—or in the vicinity of—the GPLLJ region. Therefore, on interannual time scales, it may be helpful to think of the shift in the moisture source distribution (Fig. 4b) as an intermediate case between 1) synoptic time scales, where the shift to oceanic moisture sources is more pronounced and 2) the long-term equilibrium case discussed here, where an intensification of the time-mean moisture source distribution is expected.

Future work could build upon this study by testing whether the magnitude of precipitation anomalies in the Midwest scales with "upstream" changes in specific humidity (e.g., in the Gulf of Mexico) as opposed to local changes in specific humidity, and to what extent this depends on the time scale considered. This would complement past work that found 1) fractional changes in specific humidity over land scale with the fractional increase over the corresponding oceanic source regions (Byrne and O'Gorman 2018; Chadwick et al. 2016) and 2) the fraction of time-mean precipitation originating from oceanic moisture sources increases as the planet warms

(Benedict et al. 2020; Gimeno et al. 2020; Findell et al. 2019). This "upstream" perspective may also be useful for understanding projected increases in precipitation variability with climate change (Bukovsky et al. 2017; Pendergrass et al. 2017), particularly in regions with large horizontal humidity gradients where horizontal moisture transport is important, and would complement existing explanations based on local changes in specific humidity and vertical velocity (Zhang et al. 2021; Pendergrass and Gerber 2016).

Future work should also consider the impact of changes in circulation variability that may affect precipitation in the Midwest. This may include, for example, reduced amplitude and poleward shift of the synoptic waves associated with daily GPLLJ anomalies (cf. Fig. 6) and increasing intensity of the North American monsoon (which tends to inhibit precipitation in the Midwest). Improved understanding of current and future NASH variability would be useful because the NASH's western extent is a strong predictor of GPLLJ strength (Fig. S5) and because subtropical highs provide a theoretical link between monsoon systems and low-level jets (Rodwell and Hoskins 2001).

The NASH also provides a useful framework for linking synoptic anomalies to interannual variability: winter and spring NASH anomalies are strongly correlated with the North Atlantic Oscillation (NAO), which consists of a "seesaw" fluctuation in surface pressure between the NASH to the south and the Icelandic low to the north (Hurrell and Deser 2010). In turn, the NAO is closely linked to the North Atlantic storm track through eddy–mean flow interaction (Marshall et al. 2001). While the storm track is most active in winter and spring, the ocean integrates—and propagates—this high-frequency atmospheric "forcing," leading to sea surface temperature anomalies in the subtropical Atlantic in summer and fall (Penland and Hartten 2014). In turn, these relatively slowly evolving sea surface temperature anomalies, particularly in the Western Hemisphere warm pool region, influence the extent of the NASH and the strength of the GPLLJ (Krishnamurthy et al. 2015; Weaver et al. 2009; Wang and Lee 2007).

Acknowledgments. This work was supported by NASA under Grant 80NSSC22K0997, and the U.S. National Science Foundation under Grant ICER-1663704 and the Graduate Research Fellowship Program under Grant 1745302. The authors thank the European Centre for Medium-Range Weather Forecasts for making the ERA5 data available, the PRISM climate group from Oregon State University for making the PRISM data available, and the developers of the Global Land Evaporation Amsterdam Model for making the GLEAM data available. The authors also wish to thank Ruud van der Ent for making the moisture tracking model available, Laifang Li for help in setting up the model, and Paul O'Gorman for helpful comments. Constructive comments by two anonymous reviewers on an earlier version of the manuscript helped improve the study and are gratefully acknowledged.

Data availability statement. The ERA5 data used in this study can be downloaded from the Copernicus Climate Change Service's Climate Data Store (https://cds.climate.copernicus.eu), the PRISM data can be downloaded from the PRISM climate group's website (https://prism.oregonstate.edu/recent/), and the GLEAM data can be download from https://www.gleam.eu/#datasets. Code for the moisture tracking model was adapted from Ruud Van der Ent's original implementation (van der Ent 2019) and can be accessed at https://github.com/ktcarr/WAM2layers_ERA5. The output from the moisture tracking model used in this study is available from the authors upon request. Code used to reproduce the figures in this study can be accessed at https://github.com/ktcarr/gplljmidwest-moisture-sources.

APPENDIX A

Moisture Tracking Model

a. Two-layer moisture tracking model formulation

The atmospheric budget for precipitable water is given by Eq. (1). To track moisture backward from a sink region, the model weights fluxes by the ratio of tracked precipitable water to total precipitable water. Denoting tagged precipitable water as $\tilde{w}$, a one-layer version of the moisture tracking model integrates the following equation backward in time:

$$\frac{\partial \tilde{w}}{\partial t} = \frac{\tilde{w}}{w}\left[-\nabla \cdot \frac{1}{g}\int_0^{p_s} q\mathbf{u}\, dp + E\right] - \tilde{P}, \tag{A1}$$

where $\tilde{P}$ is precipitation falling in a specified sink region:

$$\tilde{P}(x, y) = \begin{cases} P, & \text{if } (x, y) \in \text{(sink region)}, \\ 0, & \text{otherwise.} \end{cases}$$

To account for vertical shear, the model used in this study splits Eq. (A1) into two layers. The equations for the two-layer model are

$$\frac{\partial \tilde{w}_2}{\partial t} = \frac{\tilde{w}_2}{w_2}[-\nabla \cdot \mathbf{Q}_2 + \kappa F_v] - \tilde{P}\left(\frac{w_2}{w_1 + w_2}\right), \tag{A2}$$

$$\frac{\partial \tilde{w}_1}{\partial t} = \frac{\tilde{w}_1}{w_1}[-\nabla \cdot \mathbf{Q}_1 - \kappa F_v + E] - \tilde{P}\left(\frac{w_1}{w_1 + w_2}\right), \tag{A3}$$

where Eqs. (A2) and (A3) correspond to the top and bottom layers, respectively, F_v is the vertical moisture flux between the two layers, κ is a dimensionless parameter used to parameterize turbulent mixing of tracked moisture between the layers, and the vertically integrated moisture flux in each layer is given by

$$\mathbf{Q}_2 = \frac{1}{g}\int_0^{p_b} q\mathbf{u}\, dp, \quad \mathbf{Q}_1 = \frac{1}{g}\int_{p_b}^{p_s} q\mathbf{u}\, dp,$$

where p_b is the pressure at the boundary between the two model layers. The boundary between model levels, p_b, is set to the eighth vertical level (after the interpolation procedure discussed in section 2a); this corresponds to a boundary pressure of about 825 hPa for a surface pressure of 1000 hPa (see Fig. S1b for a spatial plot of the climatological boundary

pressure). We set the vertical mixing parameter as $\kappa = 3$, but the results are similar for $\kappa = 2$ and $\kappa = 4$; for discussion of this parameterization, see van der Ent et al. (2014). The vertical flux F_v is computed diagnostically after computing the horizontal fluxes in each layer; details on this procedure are provided in the following section.

The amount of moisture that each grid cell contributes to precipitation in the sink region, denoted $\tilde{E}$, is the total evaporation weighted by the fraction of tagged moisture in the model's lower layer: $\tilde{E} = E(\tilde{w}_1/w_1)$. As part of our analysis, we integrate this tracked evaporation over different spatial regions to determine how much moisture each contributes to precipitation in the Midwest. More formally, we define the scalar quantity $\tilde{E}_M(t)$ as the integral of tracked evaporation over an arbitrary region M. That is, $\tilde{E}_M(t) = \int_M \tilde{E}(t, x, y)dx\,dy$. Using this notation, we partition the total tracked moisture into components originating over land and ocean: $\tilde{E}_{\text{global}} = \tilde{E}_{\text{land}} + \tilde{E}_{\text{ocean}}$, and further decompose the oceanic contribution into components originating from the Atlantic and Pacific: $\tilde{E}_{\text{ocean}} = \tilde{E}_{\text{Atlantic}} + \tilde{E}_{\text{Pacific}}$. To facilitate comparison with studies that have attempted to quantify the Midwest's "recycling ratio," we also compute $\tilde{E}_{\text{Midwest}}$, which is tracked moisture that evaporates within the Midwest region (outlined by the dashed white line in Fig. 1a).

b. Vertical flux estimates for the moisture tracking model

The two-layer version of the precipitable water budget can be written as

$$\frac{\partial w_2}{\partial t} = -\nabla \cdot \mathbf{Q}_2 - P\left(\frac{w_2}{w_1 + w_2}\right) + F_v + \xi_2, \tag{A4}$$

$$\frac{\partial w_1}{\partial t} = -\nabla \cdot \mathbf{Q}_1 - P\left(\frac{w_1}{w_1 + w_2}\right) + E - F_v + \xi_1, \tag{A5}$$

where ξ_j is a residual and all other terms have the same meaning as in Eqs. (A3) and (A2). Except for the residual term and F_v (the vertical flux between the layers), all terms in these equations can be computed directly from ERA5. To run the moisture tracking model, F_v is computed diagnostically. Integrating the model's top level in time, we have

$$w_2^{(t_{i+1})} - w_2^{(t_i)} = \int_{t_i}^{t_{i+1}} \frac{\partial w_2}{\partial t} dt \approx \Delta t \frac{\partial w_2}{\partial t}\bigg|_{t_i}.$$

Defining $\Delta w_2 = w_2^{(t_{i+1})} - w_2^{(t_i)}$, dividing both sides by Δt, and substituting the RHS of Eq. (A4) for $\partial w_2/\partial t$, we have

$$\frac{\Delta w_2}{\Delta t} = \left[-\nabla \cdot \mathbf{Q}_2 - P\left(\frac{w_2}{w_1 + w_2}\right) + F_v + \xi_2\right]_{t_i}. \tag{A6}$$

To simplify notation, define β_2 as the contribution from the horizontal moisture fluxes and surface fluxes:

$$\beta_2^{(i)} = \left[-\nabla \cdot \mathbf{Q}_2 - P\left(\frac{w_2}{w_1 + w_2}\right)\right]_{t_i}.$$

Substituting into Eq. (A6), dividing both sides by Δt, and dropping time indices for convenience, we obtain

$$\frac{\Delta w_2}{\Delta t} = \beta_2 + F_v + \xi_2. \tag{A7}$$

Similarly, for the bottom layer, we have

$$\frac{\Delta w_1}{\Delta t} = \beta_1 - F_v + \xi_1, \tag{A8}$$

where

$$\beta_1 = -\nabla \cdot \frac{1}{g}\int_{p_b}^{p_s} q\mathbf{u}\, dp - P\left(\frac{w_1}{w_1 + w_2}\right) + E.$$

Next, we impose the constraint that the residual in each layer is proportional to the precipitable water in each layer: $\xi_1/(\xi_1 + \xi_2) = w_1/(w_1 + w_2)$. Defining $w = w_1 + w_2$ and $\xi = \xi_1 + \xi_2$, we have $\xi_1 = (w_1/w)\xi$ and $\xi_2 = (w_2/w)\xi$. Substituting these expressions into Eqs. (A7) and (A8), we obtain a system of two equations with two unknowns, F_v and ξ:

$$\frac{\Delta w_2}{\Delta t} - \beta_2 = F_v + \frac{w_2}{w}\xi,$$

$$\frac{\Delta w_1}{\Delta t} - \beta_1 = -F_v + \frac{w_1}{w}\xi.$$

Finally, F_v and ξ are obtained by solving the linear system:

$$\begin{bmatrix} F_v \\ \xi \end{bmatrix} = \begin{bmatrix} -1 & w_1/w \\ 1 & w_2/w \end{bmatrix}^{-1} \begin{bmatrix} \Delta w_2/\Delta t - \beta_2 \\ \Delta w_1/\Delta t - \beta_1 \end{bmatrix}.$$

APPENDIX B

Reynolds Decomposition of Moisture Flux Anomalies

In this section, we provide details of the moisture flux decomposition shown in Fig. 3b.

Begin by considering some variable x. Let $\overline{x}$ denote a seasonal average, $\langle\overline{x}\rangle$ denote a climatological seasonal average, $\hat{x} = \overline{x} - \langle\overline{x}\rangle$ denote the seasonal mean's deviation from climatology, and $x' = x - \overline{x}$ denote the instantaneous deviation from the seasonal mean. Note that $\langle\hat{x}\rangle = 0$ and $\overline{x'} = 0$.

Applying these rules, the climatological seasonal-mean moisture flux can be decomposed as

$$\begin{aligned}\langle\overline{qv}\rangle &= \langle\overline{q}\,\overline{v}\rangle + \langle\overline{q'v'}\rangle \\ &= \langle\overline{q}\rangle\langle\overline{v}\rangle + \langle\hat{q}\hat{v}\rangle + \langle\overline{q'v'}\rangle.\end{aligned}$$

Then seasonal-mean anomalies can then be decomposed as

$$\begin{aligned}\overline{qv} - \langle\overline{qv}\rangle &= [\overline{q}\,\overline{v} + \overline{q'v'}] - [\langle\overline{q}\rangle\langle\overline{v}\rangle + \langle\hat{q}\hat{v}\rangle + \langle\overline{q'v'}\rangle] \\ &= [\overline{q}\,\overline{v} - \langle\overline{q}\rangle\langle\overline{v}\rangle - \langle\hat{q}\hat{v}\rangle] + [\overline{q'v'} - \langle\overline{q'v'}\rangle]. \end{aligned} \tag{B1}$$

Note that $\overline{q}\,\overline{v} = (\langle\overline{q}\rangle + \hat{q})(\langle\overline{v}\rangle + \hat{v}) = \langle\overline{q}\rangle\langle\overline{v}\rangle + \hat{q}\langle\overline{v}\rangle + \langle\hat{q}\rangle\hat{v} + \hat{q}\hat{v}$. Therefore, the first bracketed term on the RHS of Eq. (B1) can be written as

$$\overline{q}\,\overline{v} - \langle\overline{q}\rangle\langle\overline{v}\rangle - \langle\hat{q}\,\hat{v}\rangle = [\langle\overline{q}\rangle\langle\overline{v}\rangle + \hat{q}\langle\overline{v}\rangle + \langle\overline{q}\rangle\hat{v} + \hat{q}\hat{v}] - \langle\overline{q}\rangle\langle\overline{v}\rangle - \langle\hat{q}\,\hat{v}\rangle = \hat{q}\langle\overline{v}\rangle + \langle\overline{q}\rangle\hat{v} + [\hat{q}\hat{v} - \langle\hat{q}\,\hat{v}\rangle].$$

Substituting back into Eq. (B1), we obtain the desired decomposition:

$$\overline{qv} - \langle\overline{qv}\rangle = \underbrace{\langle\overline{q}\rangle\hat{v}}_{\text{Dyn.}} + \underbrace{\hat{q}\langle v\rangle}_{\text{Thermo.}} + \underbrace{[\hat{q}\hat{v} - \langle\hat{q}\,\hat{v}\rangle]}_{\text{Cov. (Seasonal)}} + \underbrace{[\overline{q'v'} - \langle\overline{q'v'}\rangle]}_{\text{Cov. (High-freq.)}}.$$

Each of these terms corresponds to one of the lines plotted in Fig. 3b.

APPENDIX C

Effect of Numerical Dissipation on Moisture Tracking Results

Here, we consider the effect of numerical dissipation on our results. Specifically, we consider how erroneous tracking of moisture across the Rocky Mountains—and overestimating the Pacific Ocean's moisture contributions to Midwest precipitation—would impact the estimated importance of moisture contributions from the Atlantic Ocean and from land.

Consider the moisture budget of a parcel advected backward in time from the Midwest to the Gulf of Mexico. For simplicity, assume a divergence-free meridional flow that is constant in time and space (note this is a reasonable approximation of the time-mean flow in the GPLLJ region). Ignoring precipitation, the tracked moisture content of a parcel changes based on the local evaporation rate; that is, $d\tilde{w}/dt = \tilde{E} = E(\tilde{w}/w)$, where $\tilde{E}$ is the tracked component of the local evaporation. Tracking backward in time, the parcel's moisture content changes according to $-d\tilde{w}/dt = -(E/w)\tilde{w}$. We crudely parameterize numerical dissipation by adding a damping term, such that $-d\tilde{w}/dt = -(E/w)\tilde{w} - \beta\tilde{w}$. Here β parameterizes the rate of numerical dissipation, such that $\beta\tilde{w}$ represents the rate at which moisture is "lost" over the topography at the western boundary. Assume $\alpha = E/w$ is constant, so the tracked moisture of the parcel evolves according to: $-d\tilde{w}/dt = -(\alpha + \beta)\tilde{w}$. Denote the moisture content of the parcel when we begin tracking as $\tilde{w}_0$; then, the moisture content of the parcel after tracking backward in time for t time units is given by $\tilde{w}(-t) = \tilde{w}_0 e^{-(\alpha+\beta)t}$. In this idealized case, the total moisture contributed by land "upwind" of the Midwest is obtained by integrating the local evaporation backward over the parcel's trajectory from the Midwest to the Gulf of Mexico:

$$\tilde{E}_{\text{Land}} = \int_{-t_0}^{0} \alpha\tilde{w}(t)dt = \int_{-t_0}^{0} \alpha\tilde{w}_0 e^{(\alpha+\beta)t}\,dt = \frac{\alpha}{\alpha+\beta}\tilde{w}_0[1 - e^{-(\alpha+\beta)t_0}].$$

Any of the parcel's remaining moisture when it reaches the Gulf of Mexico is attributed to the Atlantic Ocean:

$$\tilde{E}_{\text{Atlantic}} = \tilde{w}(-t_0) = \tilde{w}_0 e^{-(\alpha+\beta)t_0}.$$

Then, ignoring the moisture lost to the Pacific via dissipation, the ratio of the Atlantic's contribution to the total is given by

$$R = \frac{\tilde{E}_{\text{Atlantic}}}{\tilde{E}_{\text{Atlantic}} + \tilde{E}_{\text{Land}}} = \frac{\tilde{w}_0 e^{-(\alpha+\beta)t_0}}{\tilde{w}_0 e^{-(\alpha+\beta)t_0} + \frac{\alpha}{\alpha+\beta}\tilde{w}_0[1 - e^{-(\alpha+\beta)t_0}]} = \frac{1}{1 + \frac{\alpha}{\alpha+\beta}[e^{(\alpha+\beta)t_0} - 1]}. \quad \text{(C1)}$$

In the limiting case where $\beta = 0$ (no numerical diffusion), this expression for R simplifies to:

$$R = \frac{1}{1 + (e^{\alpha t_0} - 1)} = e^{-\alpha t_0} = e^{-\alpha(\Delta y/v)}. \quad \text{(C2)}$$

Here, we substitute the advective time scale to $t_0 = \Delta y/v$, where Δy is the distance from the Midwest to the Gulf of Mexico, and v is the meridional velocity associated with the GPLLJ. Equation (C2) can be interpreted as follows: if the parcel travels more slowly (corresponding to smaller v and larger t_0), it loses more moisture to land, and there is less remaining moisture when it reaches the Gulf of Mexico. In the case where $\beta \neq 0$, we have $\partial R/\partial\beta \leq 0$ (not shown), indicating that as numerical dissipation increases, the ratio of $\tilde{E}_{\text{Atl}}$ to $\tilde{E}_{\text{land}}$ *decreases*. Given that our results are likely affected by numerical dissipation, this analysis suggests that the true ratio of $\tilde{E}_{\text{Atl}}$ to $\tilde{E}_{\text{land}}$ is higher than indicated by our moisture tracking model.

REFERENCES

Abel, B. D., B. Rajagopalan, and A. J. Ray, 2022: Understanding the dominant moisture sources and pathways of summer precipitation in the southeast Prairie pothole region. *Earth Space Sci.*, **9**, e2021EA001855, https://doi.org/10.1029/2021EA001855.

Agrawal, S., C. R. Ferguson, L. Bosart, and D. A. Burrows, 2021: Teleconnections governing the interannual variability of Great Plains low-level jets in May. *J. Climate*, **34**, 4785–4802, https://doi.org/10.1175/JCLI-D-20-0451.1.

Algarra, I., J. Eiras-Barca, G. Miguez-Macho, R. Nieto, and L. Gimeno, 2019: On the assessment of the moisture transport by the Great Plains low-level jet. *Earth Syst. Dyn.*, **10**, 107–119, https://doi.org/10.5194/esd-10-107-2019.

Barandiaran, D., S.-Y. Wang, and K. Hilburn, 2013: Observed trends in the Great Plains low-level jet and associated precipitation changes in relation to recent droughts. *Geophys. Res. Lett.*, **40**, 6247–6251, https://doi.org/10.1002/2013GL058296.

Bell, G. D., and J. E. Janowiak, 1995: Atmospheric circulation associated with the Midwest floods of 1993. *Bull. Amer. Meteor. Soc.*, **76**, 681–695, https://doi.org/10.1175/1520-0477(1995)076<0681:ACAWTM>2.0.CO;2.

Benedict, I., C. C. van Heerwaarden, R. J. van der Ent, A. H. Weerts, and W. Hazeleger, 2020: Decline in terrestrial

moisture sources of the Mississippi River basin in a future climate. *J. Hydrometeor.*, **21**, 299–316, https://doi.org/10.1175/JHM-D-19-0094.1.

Brubaker, K. L., P. A. Dirmeyer, A. Sudradjat, B. S. Levy, and F. Bernal, 2001: A 36-yr climatological description of the evaporative sources of warm-season precipitation in the Mississippi River basin. *J. Hydrometeor.*, **2**, 537–557, https://doi.org/10.1175/1525-7541(2001)002<0537:AYCDOT>2.0.CO;2.

Bukovsky, M. S., R. R. McCrary, A. Seth, and L. O. Mearns, 2017: A mechanistically credible, poleward shift in warm-season precipitation projected for the U.S. Southern Great Plains? *J. Climate*, **30**, 8275–8298, https://doi.org/10.1175/JCLI-D-16-0316.1.

Burrows, D. A., C. R. Ferguson, M. A. Campbell, G. Xia, and L. F. Bosart, 2019: An objective classification and analysis of upper-level coupling to the Great Plains low-level jet over the twentieth century. *J. Climate*, **32**, 7127–7152, https://doi.org/10.1175/JCLI-D-18-0891.1.

——, ——, and L. F. Bosart, 2020: The role of upper-level coupling on Great Plains low-level jet structure and variability. *J. Atmos. Sci.*, **77**, 4317–4335, https://doi.org/10.1175/JAS-D-20-0059.1.

Byrne, M. P., and P. A. O'Gorman, 2018: Trends in continental temperature and humidity directly linked to ocean warming. *Proc. Natl. Acad. Sci. USA*, **115**, 4863–4868, https://doi.org/10.1073/pnas.1722312115.

Chadwick, R., P. Good, and K. Willett, 2016: A simple moisture advection model of specific humidity change over land in response to SST warming. *J. Climate*, **29**, 7613–7632, https://doi.org/10.1175/JCLI-D-16-0241.1.

Cook, K. H., E. K. Vizy, Z. S. Launer, and C. M. Patricola, 2008: Springtime intensification of the Great Plains low-level jet and Midwest precipitation in GCM simulations of the twenty-first century. *J. Climate*, **21**, 6321–6340, https://doi.org/10.1175/2008JCLI2355.1.

Danco, J. F., and E. R. Martin, 2018: Understanding the influence of ENSO on the Great Plains low-level jet in CMIP5 models. *Climate Dyn.*, **51**, 1537–1558, https://doi.org/10.1007/s00382-017-3970-9.

Di Luzio, M., G. L. Johnson, C. Daly, J. K. Eischeid, and J. G. Arnold, 2008: Constructing retrospective gridded daily precipitation and temperature datasets for the conterminous United States. *J. Appl. Meteor. Climatol.*, **47**, 475–497, https://doi.org/10.1175/2007JAMC1356.1.

Dirmeyer, P. A., and K. L. Brubaker, 2007: Characterization of the global hydrologic cycle from a back-trajectory analysis of atmospheric water vapor. *J. Hydrometeor.*, **8**, 20–37, https://doi.org/10.1175/JHM557.1.

——, and J. L. Kinter III, 2009: The "Maya Express": Floods in the U.S. Midwest. *Eos, Trans. Amer. Geophys. Union*, **90**, 101–102, https://doi.org/10.1029/2009EO120001.

——, and ——, 2010: Floods over the U.S. Midwest: A regional water cycle perspective. *J. Hydrometeor.*, **11**, 1172–1181, https://doi.org/10.1175/2010JHM1196.1.

Dong, J., F. Lei, and W. T. Crow, 2022: Land transpiration-evaporation partitioning errors responsible for modeled summertime warm bias in the central United States. *Nat. Commun.*, **13**, 336, https://doi.org/10.1038/s41467-021-27938-6.

Feng, Z., R. A. Houze Jr., L. R. Leung, F. Song, J. C. Hardin, J. Wang, W. I. Gustafson Jr., and C. R. Homeyer, 2019: Spatiotemporal characteristics and large-scale environments of mesoscale convective systems east of the Rocky Mountains. *J. Climate*, **32**, 7303–7328, https://doi.org/10.1175/JCLI-D-19-0137.1.

Findell, K. L., P. W. Keys, R. J. van der Ent, B. R. Lintner, A. Berg, and J. P. Krasting, 2019: Rising temperatures increase importance of oceanic evaporation as a source for continental precipitation. *J. Climate*, **32**, 7713–7726, https://doi.org/10.1175/JCLI-D-19-0145.1.

Gimeno, L., and Coauthors, 2012: Oceanic and terrestrial sources of continental precipitation. *Rev. Geophys.*, **50**, RG4003, https://doi.org/10.1029/2012RG000389.

——, R. Nieto, and R. Sorí, 2020: The growing importance of oceanic moisture sources for continental precipitation. *npj Climate Atmos. Sci.*, **3**, 27, https://doi.org/10.1038/s41612-020-00133-y.

Hasegawa, T., H. Wakatsuki, and G. C. Nelson, 2022: Evidence for and projection of multi-breadbasket failure caused by climate change. *Curr. Opin. Environ. Sustainability*, **58**, 101217, https://doi.org/10.1016/j.cosust.2022.101217.

Hersbach, H., and Coauthors, 2020: The ERA5 global reanalysis. *Quart. J. Roy. Meteor. Soc.*, **146**, 1999–2049, https://doi.org/10.1002/qj.3803.

Higgins, R. W., Y. Yao, E. S. Yarosh, J. E. Janowiak, and K. C. Mo, 1997: Influence of the Great Plains low-level jet on summertime precipitation and moisture transport over the central United States. *J. Climate*, **10**, 481–507, https://doi.org/10.1175/1520-0442(1997)010<0481:IOTGPL>2.0.CO;2.

Hurrell, J. W., and C. Deser, 2010: North Atlantic climate variability: The role of the North Atlantic Oscillation. *J. Mar. Syst.*, **79**, 231–244, https://doi.org/10.1016/j.jmarsys.2009.11.002.

Krishnamurthy, L., G. A. Vecchi, R. Msadek, A. Wittenberg, T. L. Delworth, and F. Zeng, 2015: The seasonality of the Great Plains low-level jet and ENSO relationship. *J. Climate*, **28**, 4525–4544, https://doi.org/10.1175/JCLI-D-14-00590.1.

Lavers, D. A., A. Simmons, F. Vamborg, and M. J. Rodwell, 2022: An evaluation of ERA5 precipitation for climate monitoring. *Quart. J. Roy. Meteor. Soc.*, **148**, 3152–3165, https://doi.org/10.1002/qj.4351.

Li, L., and W. Li, 2015: Thermodynamic and dynamic contributions to future changes in regional precipitation variance: Focus on the southeastern United States. *Climate Dyn.*, **45**, 67–82, https://doi.org/10.1007/s00382-014-2216-3.

——, R. W. Schmitt, C. C. Ummenhofer, and K. B. Karnauskas, 2016: Implications of North Atlantic sea surface salinity for summer precipitation over the U.S. Midwest: Mechanisms and predictive value. *J. Climate*, **29**, 3143–3159, https://doi.org/10.1175/JCLI-D-15-0520.1.

——, ——, and ——, 2018: The role of the subtropical North Atlantic water cycle in recent US extreme precipitation events. *Climate Dyn.*, **50**, 1291–1305, https://doi.org/10.1007/s00382-017-3685-y.

——, ——, and ——, 2022: Skillful long-lead prediction of summertime heavy rainfall in the US Midwest from sea surface salinity. *Geophys. Res. Lett.*, **49**, e2022GL098554, https://doi.org/10.1029/2022GL098554.

Li, W., L. Li, R. Fu, Y. Deng, and H. Wang, 2011: Changes to the North Atlantic subtropical high and its role in the intensification of summer rainfall variability in the southeastern United States. *J. Climate*, **24**, 1499–1506, https://doi.org/10.1175/2010JCLI3829.1.

Lopez, P., 2011: Direct 4D-Var assimilation of NCEP stage IV radar and gauge precipitation data at ECMWF. *Mon. Wea. Rev.*, **139**, 2098–2116, https://doi.org/10.1175/2010MWR3565.1.

Malloy, K., and B. P. Kirtman, 2022: The summer Asia–North America teleconnection and its modulation by ENSO in Community Atmosphere Model, version 5 (CAM5). *Climate Dyn.*, **5**, 2213–2230, https://doi.org/10.1007/s00382-022-06205-4.

——, and ——, 2020: Predictability of midsummer Great Plains low-level jet and associated precipitation. *Wea. Forecasting*, **35**, 215–235, https://doi.org/10.1175/WAF-D-19-0103.1.

Marshall, J., and Coauthors, 2001: North Atlantic climate variability: Phenomena, impacts and mechanisms. *Int. J. Climatol.*, **21**, 1863–1898, https://doi.org/10.1002/joc.693.

Martens, B., and Coauthors, 2017: GLEAM v3: Satellite-based land evaporation and root-zone soil moisture. *Geosci. Model Dev.*, **10**, 1903–1925, https://doi.org/10.5194/gmd-10-1903-2017.

Martineau, P., G. Chen, and D. A. Burrows, 2017: Wave events: Climatology, trends, and relationship to Northern Hemisphere winter blocking and weather extremes. *J. Climate*, **30**, 5675–5697, https://doi.org/10.1175/JCLI-D-16-0692.1.

Miralles, D. G., T. R. H. Holmes, R. A. M. De Jeu, J. H. Gash, A. G. C. A. Meesters, and A. J. Dolman, 2011: Global land-surface evaporation estimated from satellite-based observations. *Hydrol. Earth Syst. Sci.*, **15**, 453–469, https://doi.org/10.5194/hess-15-453-2011.

Mo, K. C., J. N. Paegle, and R. W. Higgins, 1997: Atmospheric processes associated with summer floods and droughts in the central United States. *J. Climate*, **10**, 3028–3046, https://doi.org/10.1175/1520-0442(1997)010<3028:APAWSF>2.0.CO;2.

Pendergrass, A. G., and E. P. Gerber, 2016: The rain is askew: Two idealized models relating vertical velocity and precipitation distributions in a warming world. *J. Climate*, **29**, 6445–6462, https://doi.org/10.1175/JCLI-D-16-0097.1.

——, R. Knutti, F. Lehner, C. Deser, and B. M. Sanderson, 2017: Precipitation variability increases in a warmer climate. *Sci. Rep.*, **7**, 17966, https://doi.org/10.1038/s41598-017-17966-y.

Penland, C., and L. M. Hartten, 2014: Stochastic forcing of north tropical Atlantic sea surface temperatures by the North Atlantic Oscillation. *Geophys. Res. Lett.*, **41**, 2126–2132, https://doi.org/10.1002/2014GL059252.

Pu, B., and R. E. Dickinson, 2014: Diurnal spatial variability of Great Plains summer precipitation related to the dynamics of the low-level jet. *J. Atmos. Sci.*, **71**, 1807–1817, https://doi.org/10.1175/JAS-D-13-0243.1.

Raymond, C., and Coauthors, 2020: Understanding and managing connected extreme events. *Nat. Climate Change*, **10**, 611–621, https://doi.org/10.1038/s41558-020-0790-4.

Roderick, M. L., F. Sun, W. H. Lim, and G. D. Farquhar, 2014: A general framework for understanding the response of the water cycle to global warming over land and ocean. *Hydrol. Earth Syst. Sci.*, **18**, 1575–1589, https://doi.org/10.5194/hess-18-1575-2014.

Rodwell, M. J., and B. J. Hoskins, 2001: Subtropical anticyclones and summer monsoons. *J. Climate*, **14**, 3192–3211, https://doi.org/10.1175/1520-0442(2001)014<3192:SAASM>2.0.CO;2.

Shapiro, A., E. Fedorovich, and S. Rahimi, 2016: A unified theory for the Great Plains nocturnal low-level jet. *J. Atmos. Sci.*, **73**, 3037–3057, https://doi.org/10.1175/JAS-D-15-0307.1.

Sudradjat, A., K. L. Brubaker, and P. A. Dirmeyer, 2003: Interannual variability of surface evaporative moisture sources of warm-season precipitation in the Mississippi River basin. *J. Geophys. Res.*, **108**, 8612, https://doi.org/10.1029/2002JD003061.

Tarek, M., F. P. Brissette, and R. Arsenault, 2020: Evaluation of the ERA5 reanalysis as a potential reference dataset for hydrological modelling over North America. *Hydrol. Earth Syst. Sci.*, **24**, 2527–2544, https://doi.org/10.5194/hess-24-2527-2020.

Ting, M., and H. Wang, 2006: The role of the North American topography on the maintenance of the Great Plains summer low-level jet. *J. Atmos. Sci.*, **63**, 1056–1068, https://doi.org/10.1175/JAS3664.1.

Trenberth, K. E., 1999a: Atmospheric moisture recycling: Role of advection and local evaporation. *J. Climate*, **12**, 1368–1381, https://doi.org/10.1175/1520-0442(1999)012<1368:AMRROA>2.0.CO;2.

——, 1999b: Conceptual framework for changes of extremes of the hydrological cycle with climate change. *Climatic Change*, **42**, 327–339, https://doi.org/10.1023/A:1005488920935.

——, and C. J. Guillemot, 1995: Evaluation of the global atmospheric moisture budget as seen from analyses. *J. Climate*, **8**, 2255–2272, https://doi.org/10.1175/1520-0442(1995)008<2255:EOTGAM>2.0.CO;2.

——, and ——, 1996: Physical processes involved in the 1988 drought and 1993 floods in North America. *J. Climate*, **9**, 1288–1298, https://doi.org/10.1175/1520-0442(1996)009<1288:PPIITD>2.0.CO;2.

——, J. T. Fasullo, and J. Mackaro, 2011: Atmospheric moisture transports from ocean to land and global energy flows in reanalyses. *J. Climate*, **24**, 4907–4924, https://doi.org/10.1175/2011JCLI4171.1.

Tuttle, J. D., and C. A. Davis, 2006: Corridors of warm season precipitation in the central United States. *Mon. Wea. Rev.*, **134**, 2297–2317, https://doi.org/10.1175/MWR3188.1.

van der Ent, R. J., 2019: WAM2layersPython. Github, accessed 20 November 2019, https://github.com/ruudvdent/WAM2layersPython.

——, and O. A. Tuinenburg, 2017: The residence time of water in the atmosphere revisited. *Hydrol. Earth Syst. Sci.*, **21**, 779–790, https://doi.org/10.5194/hess-21-779-2017.

——, ——, H. R. Knoche, H. Kunstmann, and H. H. G. Savenije, 2013: Should we use a simple or complex model for moisture recycling and atmospheric moisture tracking? *Hydrol. Earth Syst. Sci.*, **17**, 4869–4884, https://doi.org/10.5194/hess-17-4869-2013.

——, L. Wang-Erlandsson, P. W. Keys, and H. H. G. Savenije, 2014: Contrasting roles of interception and transpiration in the hydrological cycle—Part 2: Moisture recycling. *Earth Syst. Dyn.*, **5**, 471–489, https://doi.org/10.5194/esd-5-471-2014.

Wang, C., and S.-k. Lee, 2007: Atlantic warm pool, Caribbean low-level jet, and their potential impact on Atlantic hurricanes. *Geophys. Res. Lett.*, **34**, L02703, https://doi.org/10.1029/2006GL028579.

Wang, S.-Y., and T.-C. Chen, 2009: The late-spring maximum of rainfall over the U.S. central Plains and the role of the low-level jet. *J. Climate*, **22**, 4696–4709, https://doi.org/10.1175/2009JCLI2719.1.

Weaver, S. J., and S. Nigam, 2008: Variability of the Great Plains low-level jet: Large-scale circulation context and hydroclimate impacts. *J. Climate*, **21**, 1532–1551, https://doi.org/10.1175/2007JCLI1586.1.

——, S. Schubert, and H. Wang, 2009: Warm season variations in the low-level circulation and precipitation over the central United States in observations, AMIP simulations, and idealized SST experiments. *J. Climate*, **22**, 5401–5420, https://doi.org/10.1175/2009JCLI2984.1.

Weng, S.-P., 2000: A new perspective on the regional hydrologic cycle over North and South America. Ph.D. thesis, Iowa State University, 172 pp., https://core.ac.uk/download/pdf/38909828.pdf.

Whiteman, C. D., X. Bian, and S. Zhong, 1997: Low-level jet climatology from enhanced rawinsonde observations at a site in the southern Great Plains. *J. Appl. Meteor.*, **36**, 1363–1376, https://doi.org/10.1175/1520-0450(1997)036<1363:LLJCFE>2.0.CO;2.

Zhang, W., K. Furtado, P. Wu, T. Zhou, R. Chadwick, C. Marzin, J. Rostron, and D. Sexton, 2021: Increasing precipitation variability on daily-to-multiyear time scales in a warmer world. *Sci. Adv.*, **7**, eabf8021, https://doi.org/10.1126/sciadv.abf8021.

Zhou, W., L. R. Leung, F. Song, and J. Lu, 2021: Future changes in the Great Plains low-level jet governed by seasonally dependent pattern changes in the North Atlantic subtropical high. *Geophys. Res. Lett.*, **48**, e2020GL090356, https://doi.org/10.1029/2020GL090356.

——, ——, and J. Lu, 2022: Seasonally dependent future changes in the U.S. Midwest hydroclimate and extremes. *J. Climate*, **35**, 17–27, https://doi.org/10.1175/JCLI-D-21-0012.1.